Christian A. Philipps, Gerhard Gompper and Roland G. Winkler

**View Online**   **Export Citation**   **CrossMark**

## ARTICLES YOU MAY BE INTERESTED IN
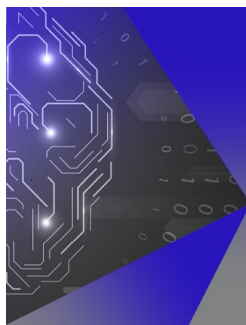
**The Journal of Chemical Physics**

AIP Publishing

# Tangentially driven active polar linear polymers—An analytical study

View Online    Export Citation    CrossMark

Christian A. Philipps,[1,2,a)] (iD) Gerhard Gompper,[1,b)] (iD) and Roland G. Winkler[1,c)] (iD)

## AFFILIATIONS

[1] Theoretical Physics of Living Matter, Institute of Biological Information Processing and Institute for Advanced Simulation, Forschungszentrum Jülich and JARA, D-52425 Jülich, Germany

[2] Department of Physics, RWTH Aachen University, 52056 Aachen, Germany

[a)] Electronic mail: c.philipps@fz-juelich.de
[b)] Electronic mail: g.gompper@fz-juelich.de
[c)] Author to whom correspondence should be addressed: r.winkler@fz-juelich.de

## ABSTRACT

The conformational and dynamical properties of isolated flexible active polar linear polymers (APLPs) are studied analytically. The APLPs are modeled as Gaussian bead-spring linear chains augmented by tangential active forces, both in a discrete and continuous representation. The polar forces lead to linear non-Hermitian equations of motion, which are solved by an eigenfunction expansion in terms of a biorthogonal basis set. Our calculations show that the polymer conformations are independent of activity. However, tangential propulsion strongly impacts the polymer dynamics and yields an active ballistic regime as well as an activity-enhanced long-time diffusive regime, which are both absent in passive systems. The polar forces imply a coupling of modes in the eigenfunction representation, in particular with the translational mode, with a respective strong influence on the polymer dynamics. The total polymer mean-square displacement on scales smaller than the radius of gyration is determined by the active internal dynamics rather than the collective center-of-mass motion, in contrast to active Brownian polymers at large Péclet numbers, reflecting the distinct difference in the propulsion mechanism.

*Published under an exclusive license by AIP Publishing.* https://doi.org/10.1063/5.0120493

## I. INTRODUCTION

Polymeric and filamentous structures are an integral part of living matter as they are fundamental for diverse molecular processes and the perpetuation of its out-of-equilibrium state.[1–3] Fueled by Adenosine Triphosphate (ATP), molecular machines, such as motor proteins and ribosomes,[4] imply an enhanced diffusional motion of biological macromolecular structures.[4–16] *In vivo*, kinesin motors couple microtubular filaments and generate forces, which affect the dynamics of the cytoskeleton network, the transport processes in the cell plasma, and the organization of the cell interior.[3,5,17–19] Similarly, nuclear ATPases such as DNA and RNA polymerases cause nonthermal fluctuations,[20–22] contribute to chromatin motion,[13,23,24] and are involved in the spatial segregation of the eukaryotic genome.[25–30]

*In vitro*, motility assays are a paradigm of active systems. Here, actin or microtubule filaments are translocated by molecular motors whose tails are anchored on a planar substrate.[31–33] Experiments reveal microtubular structures such as rotating rings in dilute systems or persistently moving large-scale swirls and bands at high filament densities.[34–37] Likewise, in mixtures of microtubules, kinesin motors, and a depletion agent, bundles emerge, which translocate due to the kinesin motors walking along the filaments.[37–39] At high enough concentration, the microtubules form a percolating active network characterized by internally driven chaotic flows, hydrodynamic instabilities, enhanced transport, and fluid mixing.[38–42]

Aside from the study of biological filamentous structures, diverse concepts are applied to obtain synthetic active colloidal polymers.[3,43–54] Here, propulsion is typically achieved by phoretic effects, based on local gradients such as electric fields (electrophoresis), concentration (diffusiophoresis), and temperature (thermophoresis).[55–64]

Various models have been proposed to elucidate the conformational and dynamical properties of active polymers and filaments and, most of the time, have been employed in computer simulations. Particular interesting aspects are the coupling between the polymer conformations, their (internal) dynamics, and the

nonequilibrium active forces. Linear polymers comprised of active Brownian particles (ABPOs)[3] exhibit an activity-induced polymer collapse, typically in two dimensions,[65–68] or swelling,[3,65,69–74] and a polymer-length-dependent suppression of phase separation.[75,76] In contrast to passive polymers, hydrodynamic interactions affect the polymer conformations, with a shrinkage for moderate and a reduced swelling for large activities.[3,77] The polymer dynamics is enhanced and new intramolecular time regimes appear.[77,78] Motor-driven filaments are typically modeled by a tangential active force.[79–90] In this case, too, computer simulations reveal strong conformational changes, typically polymer shrinkage at very high activities, and an enhanced center-of-mass (CM) dynamics, with a ballistic regime for short times and an activity-amplified long-time diffusive regime for isolated filaments.[79,82,86] Analytical calculations of semiflexible active polar ring polymers (APRPs) predict a tank-treading-like active motion along the polymer contour,[90] with the ring rotation, in agreement with experiments.[31,33] Aside from these rather generic approaches, particular realizations of the active environment are considered, such as active dipoles in the modeling of coherent chromatin motion.[28]

Computer simulations provide deep and valuable insight into the properties of individual active polymers and their collective behavior. Yet, for a detailed understanding of dynamical aspects, a theoretical model and analytical predictions are desirable. Specifically, for tangentially driven active polar linear polymers (APLPs), an elaborate model is lacking, nonetheless basic considerations have been presented.[86]

In this article, we describe consistent discrete and continuous theoretical approaches to characterize the properties of flexible APLPs. The discrete polymer is comprised of beads connected by bonds, with active forces along the bond vectors. In the continuum limit, these forces act along the local tangent of the polymer contour. The polar interactions break the polymer end-to-end symmetry, which results in non-symmetric/non-Hermitian eigenvalue problems for the linear equations of motion (EOM), which are solved by expansions into biorthogonal basis sets. In contrast to equivalent passive polymers,[91] the discrete model yields complex eigenvalues for activities exceeding a critical value. This results in a single activity-independent relaxation time and a particular dynamics determined by a superposition of time-dependent trigonometric functions with mode-dependent frequencies. The biorthogonal basis leads to a coupling of modes in the mode-amplitude correlation functions with an emerging maximum at a mode, which shifts to a higher mode number for increasing activity, whereas passive flexible polymers show an exponential decay and decoupled modes.[91,92] As a consequence, an increasing number of modes is required to ensure convergence of sums over modes in a continuous polymer description. Our approach yields polymer conformational properties, e.g., the mean-square end-to-end distance, which are unaffected by the tangential propulsion. In contrast, the dynamics is strongly activity dependent. The center-of-mass and bead mean-square displacements (MSDs) show a ballistic regime for short times and an activity-enhanced diffusive overall polymer motion for long times. The total polymer mean-square-displacement is dominated by its internal dynamics, in contrast to active Brownian polymers at very higher activities, where the center-of-mass motion prevails.[72] The long-time diffusion coefficient increases linearly with increasing propulsion

strength, in agreement with simulation results,[82] while for active Brownian polymers, it increases quadratically with activity. Furthermore, the end-to-end vector correlation function is dominated by the first relaxation time for long times, whereas multiple relaxation times contribute at short times resulting in a complex time dependence.

## II. DISCRETE MODEL—ACTIVE POLAR LINEAR BEAD-SPRING POLYMER

### A. Equations of motion

A flexible discrete linear polymer is composed of $N + 1$ beads connected by harmonic bonds. Their positions $r_j(t)$ ($j = 0, \ldots, N$) evolve in time $t$ (Fig. 1).[91] An active force $f_a R_j(t)$ is applied along the bond vector $R_j(t) = [r_j(t) - r_{j-1}(t)]$ of force density $f_a$ per bond length $l$. Then, the total active force on bead $j$ is $F_j^a(t) = f_a[R_{j+1}(t) + R_j(t)]/2 = f_a[r_{j+1}(t) - r_{j-1}(t)]/2$.[3,79] The beads' overdamped equations of motion (EOMs) are ($j = 1, \ldots, N - 1$)

$$\tilde{\gamma}\frac{d}{dt}r_0(t) = \left(\frac{f_a}{2} + \frac{3k_BT}{l^2}\right)R_1(t) + \Gamma_0(t), \tag{1}$$

$$\tilde{\gamma}\frac{d}{dt}r_j(t) = \frac{f_a}{2}[R_{j+1}(t) + R_j(t)] + \Gamma_j(t) + \frac{3k_BT}{l^2}[R_{j+1}(t) - R_j(t)], \tag{2}$$

$$\tilde{\gamma}\frac{d}{dt}r_N(t) = \left(\frac{f_a}{2} - \frac{3k_BT}{l^2}\right)R_N(t) + \Gamma_N(t), \tag{3}$$

with the bond force $F_j^b(t) = 3k_BT[R_{j+1}(t) - R_j(t)]/l^2$ and the stochastic force $\Gamma_j(t)$. The strength of the bond force, $3k_BT/l^2$, ensures that the local constraint $\langle R_j^2 \rangle = l^2$ is satisfied for all activities, which accounts for the inextensibility of a polymer in a mean-field manner,[93,94] where $T$ is the temperature, $k_B$ is the Boltzmann constant, and $L = Nl$ is the polymer contour length. In the matrix formulation of the EOMs, the polar active forces lead to a non-symmetric
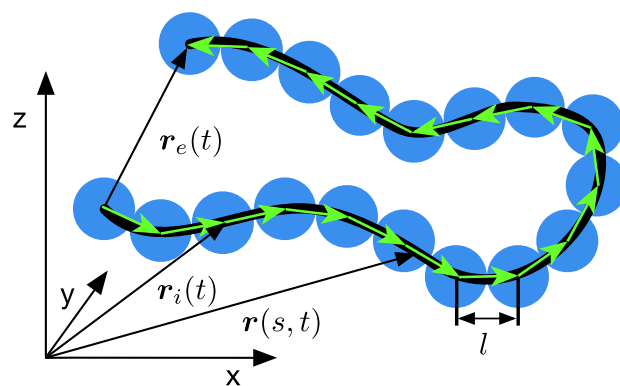


**FIG. 1.** Illustration of an active polar linear polymer. The black line indicates a continuous polymer, the blue beads the discrete one, and the green arrows the active forces along the bonds, which are tangential to the polymer in the continuum limit. Arbitrary position vectors $r_i(t)$ and $r(s, t)$ and the end-to-end vector $r_e(t)$ are shown, and the bond length $l$ is indicated.

matrix $\mathbf{M}$ [see Eqs. (S1) and (S2) of the supplementary material]. The thermal fluctuations $\boldsymbol{\Gamma}_j(t)$ are described as a stationary Gaussian and Markovian stochastic process with zero mean and the second moments,[91,92,95]

$$\langle \Gamma_{\alpha,j}(t)\Gamma_{\beta,k}(t')\rangle = 2\tilde{\gamma}k_B T\delta_{\alpha\beta}\delta_{jk}\delta(t-t'), \tag{4}$$

with the translational friction coefficient $\tilde{\gamma}$ and the Euclidean coordinates $\alpha, \beta \in \{x,y,z\}$. To characterize activity, the Péclet number

$$Pe = \frac{f_a L^2}{k_B T} \tag{5}$$

is introduced, which is the ratio between the total active energy of a polymer of length $L$ and the thermal energy.[79,90]

### B. Solution of the equations of motion

The solution of the non-symmetric (non-Hermitian) equations of motion (1)–(3) is obtained by the eigenvector expansion,

$$\boldsymbol{r}_j(t) = \sum_{m=0}^{N} \tilde{\boldsymbol{\chi}}_m(t)b_m^{(j)}, \quad \boldsymbol{\Gamma}_j(t) = \sum_{m=0}^{N} \tilde{\boldsymbol{\Gamma}}_m(t)b_m^{(j)}, \tag{6}$$

with the eigenvectors $\boldsymbol{b}_m = (b_m^{(0)},\ldots,b_m^{(N)})^T$ of the non-symmetric matrix $\mathbf{M}$ [Eq. (S2)]. A biorthogonal basis set is formed together with the adjoint eigenvectors $\boldsymbol{b}_m^{\dagger} = (b_m^{(0)\dagger},\ldots,b_m^{(N)\dagger})^T$ of the transposed matrix $\mathbf{M}^T$. The eigenvectors are normalized such that $\boldsymbol{b}_m^{\dagger} \cdot \boldsymbol{b}_n = \delta_{mn}$.[95] Explicitly, the eigenvectors are given by

$$b_m^{(j)} = \sqrt{\frac{2}{N+1}} \frac{e^{-dj}}{\sqrt{(1-r_d^2)\sin^2 \tilde{k}_m + (r_d - \lambda_m/2)^2}}$$
$$\times \left[\sqrt{1-r_d^2}\sin \tilde{k}_m \,\cos(\tilde{k}_m j) + (r_d - \lambda_m/2)\sin(\tilde{k}_m j)\right], \tag{7}$$

$$b_m^{(j)\dagger} = e^{2dj}b_m^{(j)}, \quad m \in \mathbb{N}_0, \tag{8}$$

$$b_0^{(j)} = \sqrt{\frac{\sinh(d)}{e^{dN}\sinh(d(N+1))}}, \tag{9}$$

$$d = \ln\left(\sqrt{1+r_d}/\sqrt{1-r_d}\right), \quad r_d < 1, \tag{10}$$

$$d = \ln\left(\sqrt{1+r_d}/\sqrt{r_d-1}\right) - i\frac{\pi}{2}, \quad r_d > 1, \tag{11}$$

with the wave numbers $\tilde{k}_m = m\pi/(N+1)$, the abbreviation

$$r_d = \frac{Pe}{6N^2}, \tag{12}$$

and the eigenvalues

$$\tilde{\xi}_m = \frac{N^2\tilde{\gamma}}{\pi^2\tilde{\tau}_R}\lambda_m = \frac{2N^2\tilde{\gamma}}{\pi^2\tilde{\tau}_R}\left[1 - \sqrt{1-r_d^2}\cos \tilde{k}_m\right], \quad \tilde{\xi}_0 = 0, \tag{13}$$

in terms of the relaxation time $\tilde{\tau}_R = \tilde{\gamma}L^2/(3\pi^2 k_B T)$ of a flexible passive polymer.[91,92] The eigenvalues $\tilde{\xi}_m$ can be complex for $r_d > 1$;

however, only conjugate complex pairs, $\tilde{\xi}_m = \tilde{\xi}_{N+1-m}^*$, appear in the eigenvector expansion, which implies real position vectors $\boldsymbol{r}_j(t)$ and random forces $\boldsymbol{\Gamma}_j(t)$ (Sec. S-II of the supplementary material).

Insertion of the expansion (6) into the EOMs (1)–(3) yields the equations for the mode amplitudes

$$\tilde{\gamma}\frac{d}{dt}\tilde{\boldsymbol{\chi}}_m(t) = -\tilde{\xi}_m\tilde{\boldsymbol{\chi}}_m(t) + \tilde{\boldsymbol{\Gamma}}_m(t). \tag{14}$$

In the stationary state, their solutions are

$$\tilde{\boldsymbol{\chi}}_m(t) = \frac{1}{\tilde{\gamma}}e^{-\tilde{\xi}_m t/\tilde{\gamma}}\int_{-\infty}^{t} e^{\tilde{\xi}_m t'/\tilde{\gamma}}\tilde{\boldsymbol{\Gamma}}_m(t')dt', \tag{15}$$

$$\tilde{\boldsymbol{\chi}}_0(t) = \tilde{\boldsymbol{\chi}}_0(0) + \frac{1}{\tilde{\gamma}}\int_0^{t}\tilde{\boldsymbol{\Gamma}}_0(t')dt'. \tag{16}$$

As long as $r_d < 1$, $\tilde{\xi}_m \in \mathbb{R}$ and Eq. (14) describes relaxation processes with the relaxation times

$$\tilde{\tau}_m = \frac{\tilde{\gamma}}{\tilde{\xi}_m} = \frac{\pi^2}{2N^2}\frac{\tilde{\tau}_R}{(1-\sqrt{1-r_d^2}\cos \tilde{k}_m)}. \tag{17}$$

In the case of $r_d > 1$, the $\tilde{\xi}_m$ are complex with the single mode-independent relaxation time $\tau$ and mode-dependent frequencies $\omega_m$, which, via $\tilde{\xi}_m = \xi_m^R + i\xi_m^I = \tilde{\gamma}/\tau - i\tilde{\gamma}\omega_m$, are given by

$$\tau = \frac{\pi^2}{2N^2}\tilde{\tau}_R, \quad \omega_m = \frac{2N^2}{\pi^2}\frac{1}{\tilde{\tau}_R}\sqrt{r_d^2-1}\cos \tilde{k}_m. \tag{18}$$

For $N$ even, there is one real eigenvalue, $\tilde{\xi}_0 = 0$, whereas for $N$ odd, the additional real eigenvalue $\tilde{\xi}_{(N+1)/2} = \tilde{\gamma}/\tau$ is present.

The consequences of the spectrum of complex eigenvalues on the APLP dynamics cannot as straightforwardly be interpreted as that for real eigenvalues only since the solution of the equations of motion is a superposition of many eigenfunctions.

## III. CONTINUOUS MODEL—TANGENTIALLY PROPELLED POLAR LINEAR POLYMER

### A. Equation of motion

In the continuum limit of a flexible linear polymer,[91,93,94] the equation of motion of the APLP is

$$\gamma\frac{\partial}{\partial t}\boldsymbol{r}(s,t) = f_a\frac{\partial}{\partial s}\boldsymbol{r}(s,t) + 3pk_B T\frac{\partial^2}{\partial s^2}\boldsymbol{r}(s,t) + \boldsymbol{\Gamma}(s,t) \tag{19}$$

for $pL \gg 1$, where $p$ is related to the polymer persistence length $l_p$ via $p = 1/(2l_p)$.[93,94,96] Here, $s$ is the contour variable ($s \in [0,L]$), $\gamma$ is the friction coefficient per length, and $\boldsymbol{\Gamma}(s,t)$ is a stationary, Gaussian, and Markovian stochastic process of zero mean and the second moments[91]

$$\langle \boldsymbol{\Gamma}(s,t)\cdot\boldsymbol{\Gamma}(s',t')\rangle = 6\gamma k_B T\delta(s-s')\delta(t-t'). \tag{20}$$

Equation (19) has to be solved with the free-end boundary conditions $\partial \boldsymbol{r}(s,t)/\partial s = 0$ at $s = 0, L$.

As for the discrete polymer, the strength of the bond force $3pk_BT$ ensures that the global mean-field constraint

$$L = \int_0^L \left\langle \left( \frac{\partial \mathbf{r}(s)}{\partial s} \right)^2 \right\rangle ds \qquad (21)$$

of polymer inextensibility is satisfied.

## B. Solution of the EOM—Eigenfunction expansion

The solution of the non-Hermitian equation (19) is obtained by the eigenfunction expansion

$$\mathbf{r}(s,t) = \sum_{m=0}^{\infty} \boldsymbol{\chi}_m(t)\phi_m(s), \quad \boldsymbol{\Gamma}(s,t) = \sum_{m=0}^{\infty} \boldsymbol{\Gamma}_m(t)\phi_m(s), \qquad (22)$$

in terms of a biorthogonal basis $\{\phi_m, \phi_m^\dagger; \; m \in \mathbb{N}_0\}$, following as solution of the two eigenvalue equations

$$\left( f_a \frac{\partial}{\partial s} + 3pk_BT \frac{\partial^2}{\partial s^2} \right) \phi_m = -\xi_m \phi_m, \qquad (23)$$

$$\left( -f_a \frac{\partial}{\partial s} + 3pk_BT \frac{\partial^2}{\partial s^2} \right) \phi_m^\dagger = -\xi_m \phi_m^\dagger. \qquad (24)$$

The eigenfunctions are normalized such that

$$\int_0^L \phi_m^\dagger(s)\phi_n(s)ds = \delta_{mn}. \qquad (25)$$

The free-end boundary conditions for $\mathbf{r}(s,t)$ lead to the conditions

$$\left[ \frac{d}{ds}\phi_m(s) \right]_{s=0,L} = 0, \qquad (26)$$

$$\left[ -2r_c \frac{\pi}{L} \phi_m^\dagger(s) + \frac{d}{ds}\phi_m^\dagger(s) \right]_{s=0,L} = 0 \qquad (27)$$

for the eigenfunctions. Note the distinct boundary conditions for the adjoint eigenfunction. Here, the abbreviation

$$r_c = \frac{Pe}{6\pi pL} \qquad (28)$$

is introduced. Explicitly, the eigenfunctions and adjoint ones are obtained as $(m \geq 1)$

$$\phi_m(s) = \sqrt{\frac{2}{L}} \frac{e^{-\pi r_c s/L}}{\sqrt{m^2 + r_c^2}} [m \cos(k_m s) + r_c \sin(k_m s)], \qquad (29)$$

$$\phi_m^\dagger(s) = e^{2\pi r_c s/L} \phi_m(s), \quad m \in \mathbb{N}_0, \qquad (30)$$

$$\phi_0 = \sqrt{\frac{\pi r_c}{L e^{\pi r_c} \sinh(\pi r_c)}}, \qquad (31)$$

with the wave numbers $k_m = m\pi/L$. The real eigenvalues are given by

$$\xi_m = \frac{\gamma}{\tau_R} (m^2 + r_c^2), \qquad (32)$$

with the relaxation time $\tau_R = \gamma L^2/(3\pi^2 pk_BT)$ of a flexible passive polymer.[91] The exponential decay along the polymer contour in

Eq. (29) unveils the head-tail symmetry breaking due to the polarity of the driving force.

The equations for the mode amplitudes $\boldsymbol{\chi}_m(t)$ and their solutions exhibit the same structure as in the discrete model, Eqs. (14)–(16), but with the distinct relaxation times,

$$\tau_m = \frac{\gamma}{\xi_m} = \frac{\tau_R}{m^2 + r_c^2}. \qquad (33)$$

In the following, results of the continuous with those of the discrete polymer model are compared, where the continuous description corresponds to the discrete one for $pL = N \gg 1$, $p = 1/l$, and $\gamma = \tilde{\gamma}/l$.

## IV. CONFORMATIONAL PROPERTIES

The conformational properties of the polymers are determined by the relaxation times and the mode amplitudes.

### A. Eigenvalue spectrum

Figure 2 illustrates the dependence of the eigenvalues of the discrete polymer model [Eq. (13)] on the Péclet number for various modes. In the interval $0 \leq Pe/(6N^2) \leq 1$, the eigenvalues $\tilde{\xi}_m$ are real, determining relaxation times $\tilde{\tau}_m$, and they increase/decrease with increasing $Pe$. For $Pe/(6N^2) > 1$, the complex eigenvalues are given by the real part $\xi_m^R = \tilde{\gamma}/\tau$ [Eq. (18)], with the mode-independent relaxation time $\tau$, and the imaginary part $\xi_m^I = -\tilde{\gamma}\omega_m$, with the frequencies $\omega_m$ [Eq. (18)]. These frequencies increase for modes $m \leq (N+1)/2$ and decrease for $m \geq (N+1)/2$ with increasing $Pe$. As long as $\tilde{k}_m = m\pi/(N+1) \ll 1$ and $Pe/(6N^2) \ll 1$, the eigenvalues of the discrete and continuous polymer model agree with each other, as reflected by the modes $m = 1$ and $m = 100$ in Fig. 2. For large $m$ and $Pe/(6N^2)$, the eigenvalue spectra differ due to discretization effects.
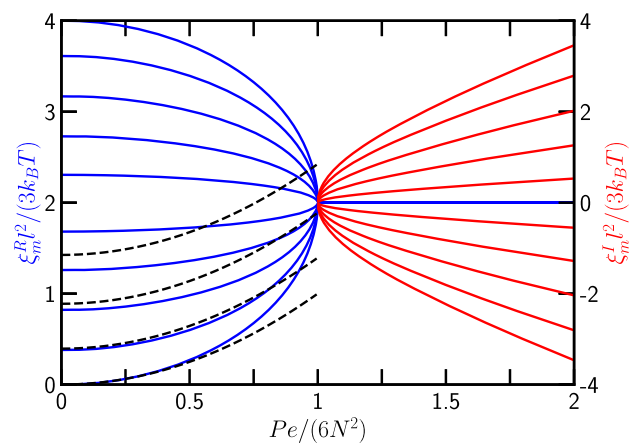


**FIG. 2.** Normalized eigenvalues $\tilde{\xi}_m$ as a function of the scaled activity $Pe/(6N^2)$ for the modes $m \in \{1, 100, 150, 190, 225, 275, 310, 350, 400, 500\}$ (bottom to top) of a discrete polymer model of length $L/l = N = 500$. The left axis corresponds to the real part (blue) and the right axis to the imaginary part (red) of the eigenvalues (13). The black dashed lines indicate the eigenvalues $\xi_m$ [Eq. (32)] of the continuous polymer model for the modes $m \in \{1, 100, 150, 190\}$ (bottom to top) and $pL = N$.

The fundamental differences in the eigenvalue spectra for $Pe/(6N^2) > 1$ reflect the distinctiveness of a discrete and a continuous polymer model. The difference equations for the eigenvalues and eigenvectors of the discrete model provide other solutions than the eigenvalue equations of the continuum approach since the latter requires a smooth and infinitesimal change of the eigenfunctions as the contour variable $s$ varies, whereas the difference equations allow only for finite discrete changes.
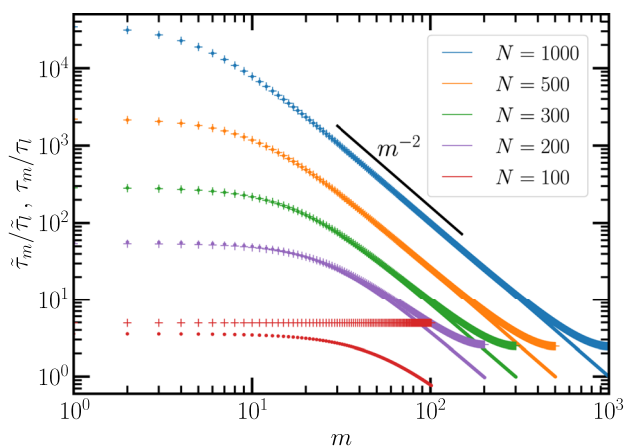
### B. Relaxation times

The relaxation times $\tilde{\tau}_m = \tilde{\gamma}/\tilde{\xi}_m$ of discrete APLPs are presented and compared with those of continuous APLPs in Fig. 3. In a passive polymer, $\tilde{\tau}_m/\tilde{\tau}_R \sim \tau_m/\tau_R \sim 1/m^2$ for $m > 1$ and $m\pi/(N+1) \ll 1$, i.e., the relaxation times decrease quadratically with increasing mode number.[92] This is no longer the case for $Pe \gg 1$, where the relaxation times assume a progressively extended plateau at small $m \geq 1$ with increasing $Pe$, as is apparent from Eq. (33).

As long as the polymers are sufficiently long such that $Pe/(6N^2) \lesssim 0.1$, the relaxation times of the discrete model closely agree with those of the continuous polymer model, except of the expected discretization discrepancies for large mode numbers. Deviations at small $m$ appear for $Pe/(6N^2) > 0.4$ and are most pronounced for $Pe/(6N^2) > 1$, where there is only one mode-independent relaxation time $\tau = \tilde{\gamma}l^2/(6k_BT)$ for the discrete polymer model (Fig. 3). In contrast, the relaxation times of the continuous polymer model $\tau_m$ [Eq. (33)] are proportional to $Pe^{-2}$ for $Pe/(6\pi pL) \gg m$ and decrease with increasing Péclet number.

### C. Correlation functions of mode amplitudes

For the discrete polymer model, the stationary-state time correlation functions of the mode amplitudes, obtained from Eqs. (15) and (16), are ($m, n \geq 1$)

$$\langle \tilde{\boldsymbol{\chi}}_m(t) \cdot \tilde{\boldsymbol{\chi}}_n(t') \rangle = \frac{6k_BT}{\tilde{\xi}_m + \tilde{\xi}_n} e^{-\tilde{\xi}_x|t-t'|/\tilde{\gamma}} \, \boldsymbol{b}_m^\dagger \cdot \boldsymbol{b}_n^\dagger, \qquad (34)$$



**FIG. 3.** Normalized relaxation times of the discrete, $\tilde{\tau}_m/\tilde{\tau}_l$ (crosses), and the continuous polymer model, $\tau_m/\tau_l$ (dots), as a function of the mode number $m$ for the Péclet number $Pe = 10^5$ and various number of beads as indicated in the legend. The normalization factor is $\tau_l = \tilde{\gamma}l^2/(3\pi^2 k_BT) = \tilde{\tau}_R/N^2$, also for the continuous polymer with $pL = N$. The black line indicates the quadratic power law decay.

where $\tilde{\xi}_x = \tilde{\xi}_m$ for $t > t'$ and $\tilde{\xi}_x = \tilde{\xi}_n$ for $t < t'$. Correlation functions comprising the mode $m = 0$ are given by

$$\langle \tilde{\boldsymbol{\chi}}_m(t) \cdot \tilde{\boldsymbol{\chi}}_0(t') \rangle = \frac{6k_BT\tilde{\tau}_m}{\tilde{\gamma}} \, \boldsymbol{b}_m^\dagger \cdot \boldsymbol{b}_0^\dagger \begin{cases} e^{-\tilde{\xi}_m(t-t')/\tilde{\gamma}}, & t > t', \\ 1, & t \leq t', \end{cases} \qquad (35)$$

$$\langle \tilde{\boldsymbol{\chi}}_0(t) \cdot \tilde{\boldsymbol{\chi}}_0(t') \rangle = \frac{6k_BT}{\tilde{\gamma}} \, \boldsymbol{b}_0^\dagger \cdot \boldsymbol{b}_0^\dagger \, t' + \tilde{\boldsymbol{\chi}}_0^2(0), \quad t \geq t' \geq 0. \qquad (36)$$

For the continuous polymer model, the stationary-state time correlation functions of the mode amplitudes are ($m, n \geq 1$)

$$\langle \boldsymbol{\chi}_m(t) \cdot \boldsymbol{\chi}_n(t') \rangle = \frac{6k_BT}{\xi_m + \xi_n} e^{-\xi_x|t-t'|/\gamma} \int_0^L \phi_m^\dagger(s)\phi_n^\dagger(s)\,ds. \qquad (37)$$

Spatial integration yields

$$\langle \boldsymbol{\chi}_m(t) \cdot \boldsymbol{\chi}_n(t') \rangle$$
$$= \frac{8r_c L^3}{\pi^3 \, pL} \frac{mn(-1 + (-1)^{m+n}e^{2\pi r_c})}{[(m-n)^2 + 4r_c^2][(m+n)^2 + 4r_c^2]\sqrt{m^2 + r_c^2}\sqrt{n^2 + r_c^2}}$$
$$\times e^{-|t-t'|/\tau_m}, \qquad (38)$$

$$\langle \boldsymbol{\chi}_m(t) \cdot \boldsymbol{\chi}_0(t') \rangle$$
$$= \frac{4r_c L^3}{\pi^3 e^{\pi r_c/2} pL} \sqrt{\frac{2\pi r_c}{\sinh(\pi r_c)}} \frac{m(-1 + (-1)^m e^{3\pi r_c})}{(m^2 + r_c^2)^{3/2}(m^2 + 9r_c^2)}$$
$$\times \begin{cases} e^{-(t-t')/\tau_m}, & t > t', \\ 1, & t \leq t', \end{cases} \qquad (39)$$

$$\langle \boldsymbol{\chi}_0(t) \cdot \boldsymbol{\chi}_0(t') \rangle = \chi_0^2(0) + \frac{3k_BT}{\gamma} e^{\pi r_c} \frac{\sinh(2\pi r_c)}{\sinh(\pi r_c)} \, t', \quad t \geq t' \geq 0, \qquad (40)$$

with the abbreviation $r_c = Pe/(6\pi pL)$ [Eq. (28)]. At equal-times, $t = t'$, and for $m = n \geq 1$, the mean-square mode amplitudes are

$$\langle \boldsymbol{\chi}_m^2 \rangle = \frac{L^3}{2\pi^3 r_c pL} \frac{m^2}{(m^2 + r_c^2)^2} (e^{2\pi r_c} - 1). \qquad (41)$$
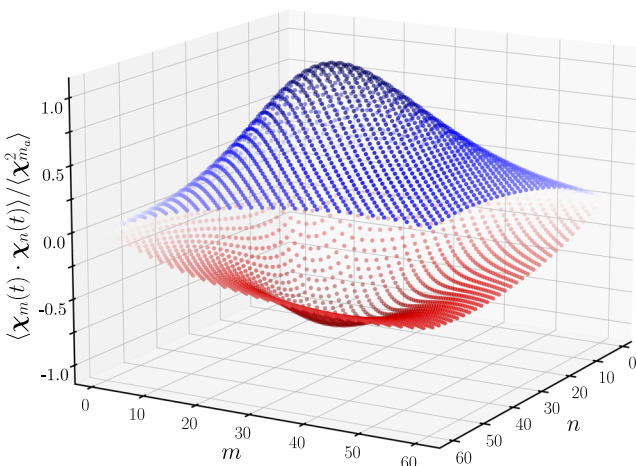
The mode-amplitude correlation functions reduce to those of a passive system in the limit of $Pe = 0$.[91] In strong contrast to the passive case, the non-Hermitian nature of the equations of motion of the APLPs implies a coupling of the mode amplitudes for $Pe > 0$. Not only couple the modes with $m \neq n, m, n \geq 1$, but also the mode $m = 0$, which describes the center-of-mass translation motion in case of a passive polymer. Such a coupling of modes was assumed in Ref. 97 to describe the broken detailed balance in the internal dynamics of semiflexible polar filaments.

Figure 4 depicts mean-square mode amplitudes for discrete and continuous APLPs [Eqs. (34) and (41)]. In the limit of $Pe \to 0$ (bottom curve), the well-known dependence $\langle \chi_m^2 \rangle \sim 1/m^2$ of passive flexible polymers is obtained,[91,92] with discretization differences at large $m$. With increasing $Pe$, gradually a maximum appears, $\langle \chi_{m_a}^2 \rangle$, which shifts to larger $m$ with increasing $Pe$. The relaxation times in the vicinity of the maximum, corresponding to the mode number
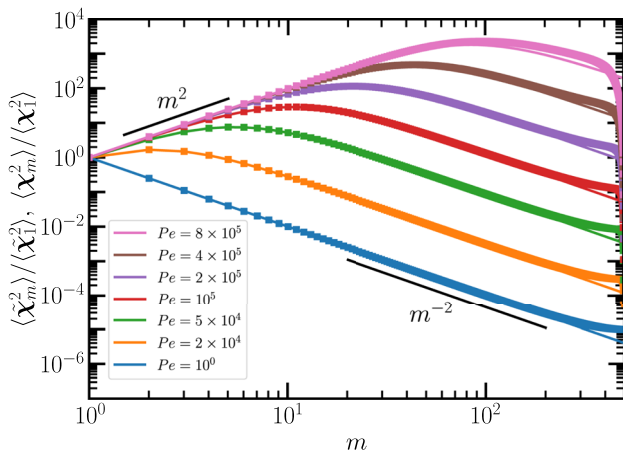
**FIG. 4.** Normalized stationary-state mean-square mode amplitudes $\langle\tilde{\chi}_m^2\rangle$ for discrete (squares) and $\langle\chi_m^2\rangle$ for continuous (lines) APLPs as a function of the mode number $m$ for various Péclet numbers $Pe$ as indicated in the legend (increasing from bottom to top) and $N = pL = 500$. $\langle\tilde{\chi}_1^2\rangle$ and $\langle\chi_1^2\rangle$ are the mean-square mode amplitudes for the mode $m = 1$, respectively. The black lines indicate quadratically increasing and decreasing power laws.

$m_a = \text{Integer}[Pe/(6\pi pL)]$, determine the APLP dynamics because they yield the largest contribution in the sum over modes in terms of the correlation functions. Below the maximum value $m_a$, the mean-square mode amplitudes increase as $\langle\tilde{\chi}_m^2\rangle \sim \langle\chi_m^2\rangle \sim m^2$ for $m \ll m_a$, and for $m > m_a$, they decrease as $\langle\tilde{\chi}_m^2\rangle \sim \langle\chi_m^2\rangle \sim m^{-2}$. The full dependence of $\langle\chi_m(t) \cdot \chi_n(t)\rangle$ on the mode numbers $m$ and $n$ is shown in Fig. 5. The values of the correlations are arranged on two "bell-shaped" surfaces, corresponding to even and odd mode numbers. This demonstrates the strong coupling between the modes and, most importantly, the presence of negative correlations.



**FIG. 5.** Normalized stationary-state mode-amplitude correlations $\langle\chi_m(t) \cdot \chi_n(t)\rangle$ of a continuous APLP as a function of the mode numbers $m$ and $n$ for $Pe = 1.9 \times 10^5$ and $pL = 500$. The normalization factor $\langle\chi_{m_a}^2\rangle$ is the maximum of $\langle\chi_m^2\rangle$ determined by the mode $m_a = 20$. The correlations $\langle\chi_m(t) \cdot \chi_n(t)\rangle$ are arranged on two "bell-shaped" surfaces, with positive (blue) and negative (red) values, respectively.

The non-Hermitian nature of the equations of motion of the APLPs leads to a tight coupling of the various modes, implying substantial deviations to the mode correlation functions of passive polymers.[91,92] Specifically, the maximum at $m_a$ for $Pe/(6\pi pL) > 1$ implies that the relaxation behavior of macroscopic quantities is typically no longer determined by the largest relaxation time but rather by $\tau_m$ in the vicinity of $m \approx m_a$. Moreover, the presence of negative values of the correlations $\langle\chi_m(t) \cdot \chi_n(t)\rangle$ causes cancellation of positive contributions in sums over modes and, hence, requires summation over many modes to achieve convergence, in particular, for continuous APLPs. On the contrary, the number of modes of discrete APLPs is limited by the number of beads.

## D. Mean-square end-to-end distance, radius of gyration

With the expansions Eqs. (6) and (22) for the discrete and continuous APLPs, respectively, the numerical evaluation of the mean-square end-to-end distances yields

$$\langle\tilde{r}_e^2\rangle = \langle(\tilde{r}_N(t) - \tilde{r}_0(t))^2\rangle = Nl^2, \tag{42}$$

$$\langle r_e^2\rangle = \langle(r(L,t) - r(0,t))^2\rangle = \frac{L}{p}, \tag{43}$$

over the considered range of Péclet numbers, $0 \le Pe \le 10^8$, various $N$, and even in the case of complex eigenvalues $[Pe/(6N^2) > 1]$—identical to those of passive polymers. The double sums over modes have to be performed numerically, and for the continuous polymer, a sufficiently large number of modes has to be taken into account to achieve convergence (Sec. S-III of the supplementary material). Similarly, the radii of gyration, $\langle r_g^2\rangle = \langle r_e^2\rangle/6$, are identical with those of passive polymers, and even the mean-square bond lengths satisfy the constraints $\langle R_i^2\rangle = l^2$ for all Péclet numbers. Moreover, subsequent bond vectors are independent, i.e., $\langle R_{i+1} \cdot R_i\rangle = 0$, as applies for flexible phantom polymers.[92] Hence, within the adopted models, the polymer conformational properties of tangentially driven linear polymers are independent of propulsion.[86] This is in contrast to computer simulations of polar polymers, which predict polymer shrinkage, however, applying a different bond potential,[79,81,82] a different tangential active force,[82] as well as excluded-volume interactions.

The simulations of Ref. 82 predict a shrinkage of a discrete phantom polymer for $Pe/N^2 \gtrsim 20$—note the different description of the active tangential force in Ref. 82—and thus, a deviation from the linear $N$ dependence in Eq. (42) occurs. Although, this differs from the predictions of the present Gaussian flexible APLP model, these simulation results of the dynamics can be compared to the analytical ones as long as $Pe/N^2 \lesssim 20$, which for a polymer with $N = 500$ beads corresponds to $Pe \lesssim 5 \times 10^6$. As will be shown in Sec. V, the APLP dynamics exhibits generic activity effects for such Péclet numbers.

## V. DYNAMICAL PROPERTIES

The translational motion of polymers is characterized by the total mean-square displacement (MSD), averaged over the polymer contour, which for a continuous polymer is

$$\langle \Delta \boldsymbol{r}_{tot}^2(t) \rangle = \frac{1}{L} \int_0^L \langle (\boldsymbol{r}(s,t) - \boldsymbol{r}(s,0))^2 \rangle ds, \quad (44)$$

and comprises contributions from the center-of-mass motion, $\langle \Delta \boldsymbol{r}_{cm}^2(t) \rangle$, and the internal dynamics in center-of-mass reference frame, $\langle \Delta r^2(t) \rangle$, such that

$$\langle \Delta \boldsymbol{r}_{tot}^2(t) \rangle = \langle \Delta \boldsymbol{r}_{cm}^2(t) \rangle + \langle \Delta r^2(t) \rangle. \quad (45)$$

Analogous definitions apply for the discrete polymer model.

Primarily, analytical results for continuous flexible APLPs are presented because appearing integrals and sums can often be evaluated and approximated analytically, whereas the sums in case of discrete APLPs cannot. However, numerically, the discrete APLPs can be treated more rigorously than the continuous APLPs because the latter require summation over a huge number of modes to achieve convergence, especially at large Péclet numbers.
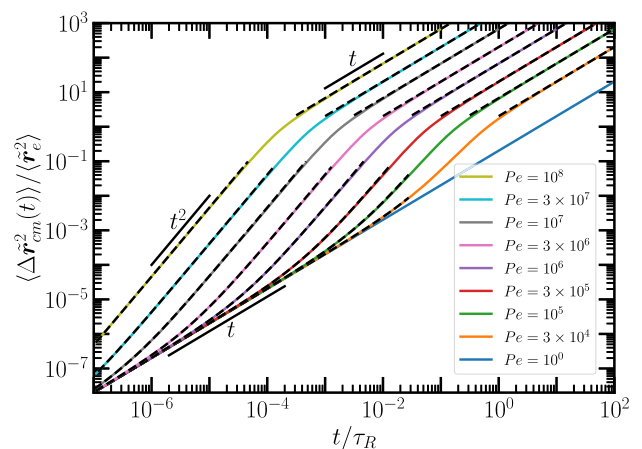
## A. Center-of-mass mean-square displacement

The calculation of the center-of-mass mean-square displacement (CM-MSD)

$$\langle \Delta \boldsymbol{r}_{cm}^2(t) \rangle = \langle (\boldsymbol{r}_{cm}(t) - \boldsymbol{r}_{cm}(0))^2 \rangle, \quad (46)$$

with $\boldsymbol{r}_{cm}(t) = \int_0^L \boldsymbol{r}(s,t)ds/L$ and $\tilde{\boldsymbol{r}}_{cm}(t) = \sum_{j=0}^N \boldsymbol{r}_j(t)/(N+1)$, respectively, for discrete and continuous APLPs yields

$$\langle \Delta \tilde{\boldsymbol{r}}_{cm}^2(t) \rangle = \frac{2L^2}{\pi^2} \frac{\coth(d(N+1))}{\coth(d)} \frac{t}{\tilde{\tau}_R} + \frac{12k_BT}{N+1} \sum_{m=1}^N \frac{\boldsymbol{b}_m^\dagger \cdot \boldsymbol{b}_0^\dagger}{\tilde{\xi}_m}$$
$$\times \boldsymbol{b}_m \cdot \boldsymbol{b}_0 \left(1 - e^{-\tilde{\xi}_m t/\tilde{\gamma}}\right) + \frac{12k_BT}{(N+1)^2} \sum_{m,n=1}^N \frac{\boldsymbol{b}_m^\dagger \cdot \boldsymbol{b}_n^\dagger}{\tilde{\xi}_m + \tilde{\xi}_n}$$
$$\times \sum_{i,j=0}^N b_m^{(i)} b_n^{(j)} \left(1 - e^{-\tilde{\xi}_m t/\tilde{\gamma}}\right), \quad (47)$$

$$\langle \Delta \boldsymbol{r}_{cm}^2(t) \rangle = 6D_R \pi r_c \coth(\pi r_c) \, t + \frac{32 r_c^3 L}{\pi^3 e^{\pi r_c} \sinh(\pi r_c) p} \sum_{m=1}^\infty \frac{m^2 \left(1 - (-1)^m e^{-\pi r_c}\right)\left(-1 + (-1)^m e^{3\pi r_c}\right)}{(m^2 + r_c^2)^3 (m^2 + 9r_c^2)} \left(1 - e^{-t/\tau_m}\right)$$
$$+ \frac{128 r_c^3 L}{\pi^5 p} \sum_{m,n=1}^\infty \frac{m^2 n^2 \left(1 - (-1)^m e^{-\pi r_c}\right)\left(1 - (-1)^n e^{-\pi r_c}\right)\left(-1 + (-1)^{m+n} e^{2\pi r_c}\right)}{[(m-n)^2 + 4r_c^2][(m+n)^2 + 4r_c^2](m^2 + r_c^2)^2(n^2 + r_c^2)^2} \left(1 - e^{-t/\tau_m}\right), \quad (48)$$

with the abbreviation $d$ of Sec. II B, $r_c$ of Eq. (28), and the diffusion coefficient $D_R = k_BT/(\gamma L)$ of a continuous passive flexible polymer.[91,92] Evidently, the non-Hermitian nature of the equations of motion implies a coupling of the translational mode ($m = 0$) with higher modes ($m \geq 1$) as well as a coupling between higher modes ($m, n \geq 1$). Thus, the CM-MSDs Eqs. (47) and (48) differ distinctively from those of passive[92] and active Brownian polymers,[71] where the CM-MSD is solely determined by the translational mode.

Figure 6 displays the CM-MSD of discrete APLPs and the comparison with the analytical results of the continuous model for various Péclet numbers. Evidently, the two representations yield the same results, and discretization effects are of minor importance for this polymer length. In the limit $Pe \to 0$, the diffusive behavior of the passive flexible polymer is found.[91,92] Clearly, three-time regimes can be identified for $Pe > 1$. Taylor expansion of Eq. (48) for short times $t/\tau_R \ll 1$ and $Pe > 0$ yields (Sec. S-IV A of the supplementary material)

$$\frac{\langle \Delta \boldsymbol{r}_{cm}^2(t) \rangle}{\langle \boldsymbol{r}_e^2 \rangle} \approx \frac{2}{\pi^2} \frac{t}{\tau_R} + \frac{Pe^2}{9\pi^4 (pL)^2} \left(\frac{t}{\tau_R}\right)^2, \quad (49)$$

with the diffusive regime of a passive polymer for $t/\tau_R \ll 18\pi^2 (pL)^2/Pe^2$ and an active ballistic regime for $t/\tau_R \gg 18\pi^2 (pL)^2/Pe^2$ and $Pe \gg 1$. Both terms in Eq. (49) are determined by the internal polymer dynamics with all modes contributing. In particular, the term linear in $t$ in Eq. (48) is canceled by a similar term resulting from the sums in Eq. (48) (Sec. S-IV A of the supplementary material). For $t/\tau_R \gg 3\pi^2 pL/Pe$, the exponential

terms, $e^{-t/\tau_m}$, in Eq. (48) are negligible, and the time dependence of the CM-MSD is entirely determined by the linear term, i.e., the APLPs exhibit diffusive motion with the activity-enhanced diffusion coefficient



**FIG. 6.** Normalized center-of-mass mean-square displacements $\langle \Delta \tilde{\boldsymbol{r}}_{cm}^2(t) \rangle$ as a function of the time $t/\tau_R$ for discrete APLPs of length $L/l = N = 500$ and various Péclet numbers $Pe$ as indicated in the legend. The blue curve for $Pe = 1$ represents the CM-MSD of a passive polymer. The black dashed lines show the approximations of the short time ballistic regime [Eq. (49)] and the long-time activity-enhanced diffusion [Eq. (50)] for continuous APLPs. The black solid lines indicate power laws.

$$\frac{D}{D_R} = \frac{Pe}{6pL} \coth\left(\frac{Pe}{6pL}\right) \approx \begin{cases} 1 + \frac{1}{3}\left(\frac{Pe}{6pL}\right)^2, & Pe \ll 1, \\ \frac{Pe}{6pL}, & Pe \gg 1, \end{cases} \quad (50)$$

where $D_R = k_B T/(\gamma L)$.[86] Note that the diffusion coefficient [Eq. (50)] follows from the correlation function of Eq. (40) for the mode $m = 0$ and, hence, is determined by the thermal fluctuations.

Similarly, the calculations for the discrete polymer model yield

$$\frac{D}{D_R} = \begin{cases} \dfrac{N\coth(d(N+1))}{\coth(d)}, & \dfrac{Pe}{6N^2} < 1, \\ \dfrac{N\tanh(\bar{d}(N+1))}{\tanh(\bar{d})}, & \dfrac{Pe}{6N^2} > 1, \quad N \text{ even}, \\ \dfrac{N\coth(\bar{d}(N+1))}{\tanh(\bar{d})}, & \dfrac{Pe}{6N^2} > 1, \quad N \text{ odd}, \end{cases} \quad (51)$$

with $\bar{d} = \ln(\sqrt{Pe + 6N^2}/\sqrt{Pe - 6N^2})$. For the discrete APLP model, there is a pronounced odd–even effect in terms of the bond number $N$ as long as $Pe/(6N^2) > 1$ and $\bar{d}(N + 1) \ll 1$. In the case $Pe/(6N^2) \gg 1$, Taylor expansion yields

$$\frac{D}{D_R} \approx \begin{cases} N(N+1), & N \text{ even}, \\ \dfrac{Pe^2}{36N^3(N+1)}, & N \text{ odd}. \end{cases} \quad (52)$$

Hence, for $N$ even, the long-time diffusion coefficient is independent of activity, whereas for $N$ odd, $D$ shows a strong dependence on $Pe$. This is confirmed by numerical evaluation of Eq. (S40) of the supplementary material. The manifestation of the odd–even difference requires large activities $Pe/(6N^3) \gg 1$, with the diffusion coefficient for odd $N$ strongly exceeding that for even $N$. We attribute this difference to a (partial) cancellation of active forces in case of an even number of bonds, whereas such a cancellation is not possible for an odd number. Figure S1 of the supplementary material provides an example for the CM-MSD of polymers of length $L/l = N = 50$ and $N = 51$. It illustrates the odd–even effect on the long-time diffusive motion as well as the emergence of oscillations on shorter time scales (see also movies M1-N50, M2-N51, and M2-N50-cm). The oscillations are a consequence of the propulsive motion of the APLPs, which resembles to some extent the tank-treading motion of APRPs.[90] At very large Péclet numbers, this occurs because the active motion along the polymer contour is faster than the relaxation of the polymer conformation. Without the long-time diffusive contribution to the MSD [first term on the right-hand side of Eq. (47)], the polymer center-of-mass is "confined" in a sphere of radius $(\langle r_g^2 \rangle)^{1/2}$, which it traverses very fast, approaching repeatedly previous positions. The rapid turning is reflected in the autocorrelation function of the polymer end-to-end vector, which also exhibits oscillations, as illustrated in Fig. S3.

In contrast, as long as $\bar{d}(N+1) \gg 1$, $D/D_R \approx N/\tanh\bar{d}$ is independent of the odd–even nature of $N$, and $D/D_R \approx Pe/(6N)$ for $Pe/(6N^2) \gg 1$, with a $Pe$ and $N$ dependence comparable to that of Eq. (50).

The diffusion coefficient in Eq. (50) increases linearly with $Pe$ for $Pe \gg 1$.[86] This agrees with simulations of active filaments in two[79] and three[82,98] dimensions. Moreover, the long-time diffusion coefficient $D \approx D_R Pe/(6pL) = f_a/(6\gamma p) = f_a l^2/(6\tilde{\gamma})$ is independent of the polymer length and depends linearly on the activity, as

has also been found in Ref. 82. The linear $Pe$ dependence of $D$ [Eq. (50)] for $Pe \gg 1$ differs from that of the diffusion coefficient of individual active Brownian particles (ABPs) and active Brownian polymers, which exhibit a quadratic $Pe$ dependence,[3,55,63,72,99] reflecting the different underlying propulsion mechanisms (see Sec. S-VII of the supplementary material). For discrete APLPs, the active force on the center-of-mass is $\boldsymbol{F}_a^{cm} = f_a(\boldsymbol{r}_N - \boldsymbol{r}_0)/(N+1) = f_a \tilde{\boldsymbol{r}}_e/(N+1)$ and, hence, depends on the polymer conformations. In contrast, the propulsion force in ABPs and ABPOs is related to a solid-body rotation of an ABP and, in the case of ABPOs, is independent of the polymer conformations.

For shorter discrete polymers, the active diffusion with the diffusion coefficient in Eq. (50) and $1 \ll Pe \ll 6N^3$ can be considered as motion with a constant velocity $v$ along the contour of a flexible polymer. This assumption implies

$$\langle (\boldsymbol{r}_i(t) - \boldsymbol{r}_i(0))^2 \rangle = lvt \quad (53)$$
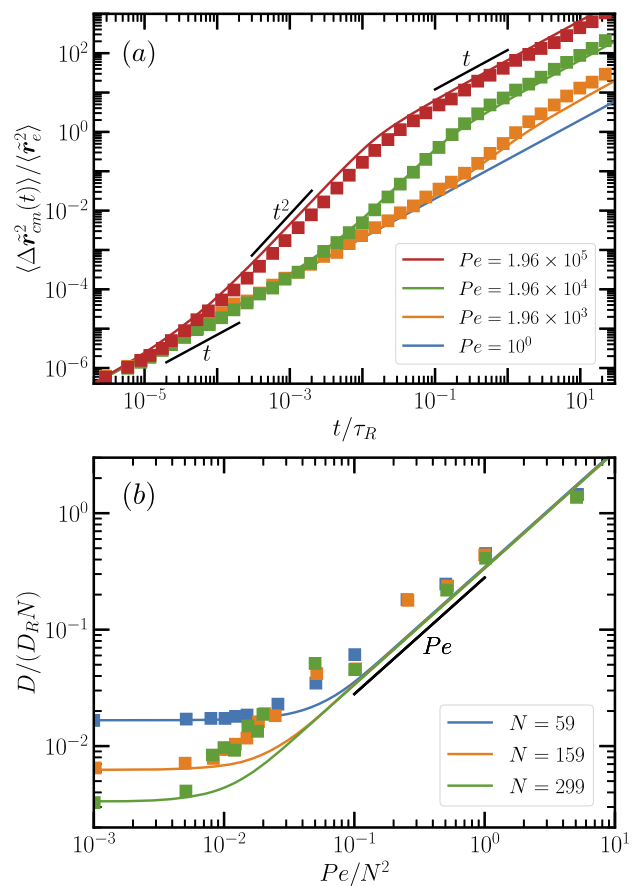


**FIG. 7.** (a) Normalized polymer center-of-mass mean-square displacements as a function of the time $t/\tau_R$ for discrete APLPs of length $L/l = N = 99$ and various Péclet numbers $Pe$ as indicated in the legend. The blue solid line for $Pe = 1$ represents the CM-MSD of a passive polymer. (b) Long-time polymer center-of-mass diffusion coefficients $D$ normalized by $D_R N = k_B T/\tilde{\gamma}$ as a function of the activity $Pe/N^2$. The symbols (squares) are simulation results for polymers with (a) 100 and (b) 50, 160, and 300 beads, taken from Ref. 82, and the lines are calculated via (a) Eq. (47) and (b) Eq. (51) for the same number of beads. The black solid lines indicate power laws for time $t$ and the Péclet number $Pe$, respectively.

for any monomer, with $v = f_a l/\tilde{\gamma} = Pe k_B T/(l\tilde{\gamma} N^2)$, and yields the diffusion coefficient $D/D_R = Pe/(6N)$ as in Eq. (50). This argument is valid as long as the ratio $L/l = N$ between the polymer length and the persistence length $[l_p = 1/(2p) = l/2]$ is not too large. It does not apply to the adopted continuum description because in that case $pL \gg 1$.

Figure 7 presents a comparison between simulation results of Ref. 82 and the analytical expression of APLPs for the polymer CM-MSD (Eq. 47) and the long-time diffusion coefficients (Eq. 51). It is important to note that the diffusion coefficient of Eq. (50) is almost identical with Eq. (51) of the discrete polymer over the considered range of Péclet numbers. The theoretical results capture the active force dependence obtained in simulations very well, both for the CM-MSD in Fig. 7(a) as well as the diffusion coefficients in Fig. 7(b). In our approach, the polymer conformations are independent of $Pe$, and thus, it does not show the shrinkage of polar polymers as observed in simulations for $Pe/N^2 > 1$,[81,82] with a corresponding reduction in the CM-MSD and $D$. In general, the theoretical curves in Fig. 7(b) are shifted toward larger $Pe$, and multiplication with a factor of $\sim 1.5$ yields better agreement, specifically for $N = 59$. This quantitative difference might originate from the different models, e.g., no self-avoidance in the presented model of APLPs, and the different implementation of the active tangential force, compare Eqs. (1)–(3) with Eq. (6) of the supplementary material of Ref. 82.

Despite that, the crossover time, $\tau_c = (\gamma/k_B T)L^3/Pe$, from the active ballistic to the active diffusive time regime, agrees with the scaling relation found by the simulations of Ref. 82.

## B. Mean-square displacement in the center-of-mass reference frame

Figure 8 presents the contour-averaged mean-square displacement of the beads of the discrete polymer model in the center-of-mass reference frame,

$$\langle \Delta \tilde{\boldsymbol{r}}^2(t) \rangle = \frac{1}{N+1} \sum_{j=0}^{N} \left\langle \left( \Delta \tilde{\boldsymbol{r}}_j(t) - \Delta \tilde{\boldsymbol{r}}_j(0) \right)^2 \right\rangle, \qquad (54)$$

with $\Delta \tilde{\boldsymbol{r}}_j(t) = \boldsymbol{r}_j(t) - \tilde{\boldsymbol{r}}_{cm}(t)$. Explicitly, it reads

$$\langle \Delta \tilde{\boldsymbol{r}}^2(t) \rangle = \frac{12 k_B T}{N+1} \sum_{m,n=1}^{N} \frac{\boldsymbol{b}_m^\dagger \cdot \boldsymbol{b}_n^\dagger}{\tilde{\xi}_m + \tilde{\xi}_n} \left( 1 - e^{-\tilde{\xi}_m t/\tilde{\gamma}} \right)$$

$$\times \left[ \boldsymbol{b}_m \cdot \boldsymbol{b}_n - \frac{1}{N+1} \sum_{i,j=0}^{N} b_m^{(i)} b_n^{(j)} \right] \qquad (55)$$

in terms of the eigenvectors [Eqs. (7) and (8)].

In the limit $Pe \to 0$, the various time regimes well-known for flexible polymers are obtained, with a linear increase in $\langle \Delta \tilde{\boldsymbol{r}}^2(t) \rangle$ with increasing time for $t/\tilde{\tau}_R \ll 1/N^2$, $\langle \Delta \tilde{\boldsymbol{r}}^2(t) \rangle \sim \sqrt{t/\tilde{\tau}_R}$ in the interval $1/N^2 < t/\tilde{\tau}_R \ll 1$, and the plateau value $\langle \Delta \tilde{\boldsymbol{r}}^2(t) \rangle = 2\langle \tilde{\boldsymbol{r}}_g^2 \rangle = \langle \tilde{\boldsymbol{r}}_e^2 \rangle/3$ for $t/\tilde{\tau}_R \gg 1$ [cf. Eqs. (42) and (43)].

With increasing activity, gradually a linear time regime appears, and $\langle \Delta \tilde{\boldsymbol{r}}^2(t) \rangle$ grows more strongly than $t^{1/2}$ of the passive polymer. The crossover time $t_c$ to the linear time regime depends on the Péclet number. As long as $Pe/(6N^2) < 1$, the continuous polymer model yields $t_c/\tau_R \approx \pi(6N/Pe)^2$, consistent with Fig. 8. For $Pe/(6N^2) > 1$, the eigenvalues $\tilde{\xi}_m$ are complex. The linear time
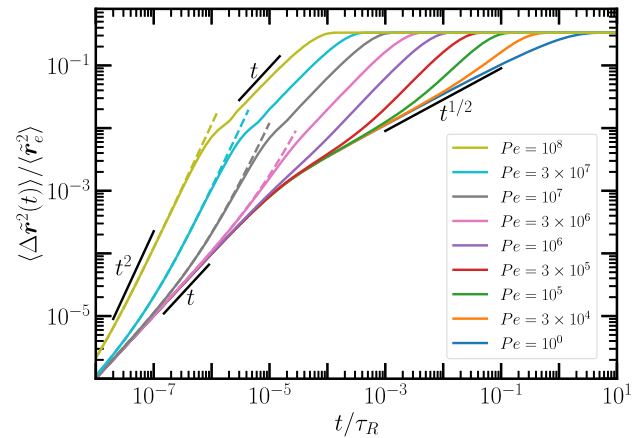


**FIG. 8.** Normalized bead mean-square displacements in the center-of-mass reference frame $\langle \Delta \tilde{\boldsymbol{r}}^2(t) \rangle$ as a function of the time $t/\tau_R$ for a discrete polymer of length $L/l = N = 500$ and various Péclet numbers $Pe$ as indicated in the legend. The colored dashed lines represent the second-order approximation of Eq. (S42). The black lines indicate power laws.
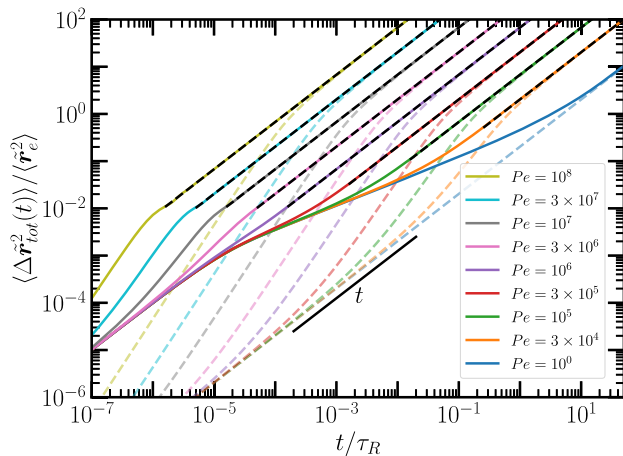
regime is determined by the difference of the $\cos(\omega_m t)$ and $\sin(\omega_m t)$ terms, which appear from the exponential $e^{i\omega_m t}$ of the imaginary part of the eigenvalue $\tilde{\xi}_m$. From the condition $\omega_1 t_c \approx 1$ for the largest frequency $\omega_1$, the crossover time $t_c/\tilde{\tau}_R \approx 3\pi^2/Pe$ is found, consistent with Fig. 8. For times $t/\tilde{\tau}_R \ll 3\pi^2/Pe$, an active quadratic time regime is present. The dashed lines in Fig. 8 represent Eq. (55) with the exponential function expanded up to second order in $\tilde{\xi}_m t/\tilde{\gamma}$. Here, the linear terms of the real and imaginary parts of $\tilde{\xi}_m$ and their product are most important and determine the time dependence. Remarkably, the MSD is real, as expected for a physical quantity, despite imaginary eigenvalues, as shown in Sec. S-II of the supplementary material. For times $t/\tilde{\tau}_R \gg \pi^2 N/Pe$, the plateau value $Nl^2/3$ is assumed, where the crossover time $t_c/\tilde{\tau}_R = \pi^2 N/Pe$ follows from the condition $Nl^2/3 = 6Dt_c$, with $D$ in Eq. (51).

As our numerical calculations show, the two terms in Eq. (S42) of the supplementary material cancel each other to some extent. This poses a major challenge in the evaluation of the sums and hampers the confirmation and interpretation of the observed linear time dependence. However, the $Pe$ dependence of the characteristic crossover time $t_c/\tilde{\tau}_R = \pi^2 N/Pe$ to the plateau regime is remarkable. This relation does not follow from the longest relaxation time, $(1 + (Pe/(6\pi N))^2)t/\tau_R \ll 1$, which is significantly smaller than $t_c/\tilde{\tau}_R$ and exhibits a stronger dependence on $Pe$, but is rather determined by the frequency $\omega_1$ in the case of $Pe/(6N^2) > 1$.

## C. Total bead mean-square displacement

The total MSD of the beads, Eqs. (44) and (45),

$$\langle \Delta \tilde{\boldsymbol{r}}_{tot}^2(t) \rangle = \frac{2L^2}{\pi^2} \frac{\coth(d(N+1))}{\coth(d)} \frac{t}{\tilde{\tau}_R}$$

$$+ \frac{12 k_B T}{N+1} \sum_{m=1}^{N} \frac{\boldsymbol{b}_m^\dagger \cdot \boldsymbol{b}_0^\dagger}{\tilde{\xi}_m} \boldsymbol{b}_m \cdot \boldsymbol{b}_0 \left( 1 - e^{-\tilde{\xi}_m t/\tilde{\gamma}} \right)$$

$$+ \frac{12 k_B T}{N+1} \sum_{m,n=1}^{N} \frac{\boldsymbol{b}_m^\dagger \cdot \boldsymbol{b}_n^\dagger}{\tilde{\xi}_m + \tilde{\xi}_n} \boldsymbol{b}_m \cdot \boldsymbol{b}_n \left( 1 - e^{-\tilde{\xi}_m t/\tilde{\gamma}} \right), \qquad (56)$$

**FIG. 9.** Normalized total bead mean-square displacements $\langle \Delta \tilde{r}_{tot}^2(t) \rangle$ (solid lines) as a function of the time $t/\tau_R$ for a discrete polymer of length $L/l = N = 500$ and various Péclet numbers $Pe$ as indicated in the legend. The dashed lines present the corresponding center-of-mass MSDs, $\langle \Delta \tilde{r}_{cm}^2(t) \rangle$. The black dashed lines indicate the active long-time diffusive regime, with the diffusion coefficient of continuous polymers [Eq. (50)]. The black solid line indicates a power law.

[see Eq. (S43) of the supplementary material] is displayed in Fig. 9. Evidently, $\langle \Delta \tilde{r}_{tot}^2(t) \rangle$ is dominated by the bead MSD in the center-of-mass reference frame up to $\langle \Delta \tilde{r}_{tot}^2(t) \rangle \approx \langle \tilde{r}_e^2 \rangle$. Strikingly, the linear time regime of $\langle \Delta \tilde{r}^2(t) \rangle$ for $t/\tilde{\tau}_R \gg \pi(6N/Pe)^2$ and $Pe/(6N^2) < 1$ and $t/\tilde{\tau}_R \gg 3\pi^2/Pe$ and $Pe/(6N^2) > 1$ joins smoothly with the respective regime in the CM-MSD, although $\langle \Delta \tilde{r}^2(t) \rangle$ assumes the plateau value $2\langle \tilde{r}_g^2 \rangle = \langle \tilde{r}_e^2 \rangle/3$, and the CM-MSD has not yet reached the long-time asymptotic value. As shown in Fig. S2 of the supplementary material, the contribution of the sums over modes $m, n \neq 0$ in Eq. (56) to $\langle \Delta \tilde{r}_{tot}^2(t) \rangle$ becomes smaller with increasing $Pe$ for $t/\tilde{\tau}_R \gg \pi(6N/Pe)^2$ and $t/\tilde{\tau}_R \gg 3\pi^2/Pe$, respectively, and the contribution of the sums over modes with $m, n \neq 0$ assumes a time-independent value much smaller than $\langle \tilde{r}_g^2 \rangle$. Thus, the total MSD is dominated by the term linear in time in Eq. (56). Contributions from the internal dynamics cancel in Eq. (56), and the share from the mode $m = 0$ prevails. At shorter times $t/\tilde{\tau}_R \ll \pi(6N/Pe)^2$ for $Pe/(6N^2) < 1$, the passive polymer total MSD is assumed. Here,

the sums over modes $m, n \neq 0$ determine the dynamics. In the case $Pe/(6N^2) > 1$ and $t/\tilde{\tau}_R \ll 3\pi^2/Pe$, cancellation of the linear terms in the sums over modes $m, n \neq 0$ yields a ballistic time regime, as for the MSD in the center-of-mass reference frame (Fig. 8).

The MSD reflects a complex interdependence of the dynamics of the active beads. The active motion along the continuously changing polymer contour implies strong correlations in the bead translational motion, specifically on shorter time scales.

Our discussion of the MSD is focused on discrete APLPs. The numerical evaluation of the sums of modes of the continuous polymer model poses major challenges since it requires summation over a huge number of modes, specifically for large $Pe$, and a high precision to compensate the large value of exponential factors containing $Pe/(6\pi pL)$. However, based on our continuum approximations of APLPs for the CM-MSD, we can confidently state that the MSD in the center-of-mass reference frame of the continuous polymer model agrees with that of a discrete polymer model as long as $Pe \lesssim 10^6$ ($Pe/(6N^2) < 1$) and $t/\tilde{\tau}_R \gtrsim 1/N^2$.

Section S-VII of the supplementary material presents a comparison between the total bead MSD of APLPs and ABPOs. The dynamics of APLPs is faster than that of ABPOs over the considered range of Péclet numbers. However, on time scales larger than the crossover time from the ballistic to the linear time dependence of the MSD of APLPs, $t/\tilde{\tau}_R \gg 3\pi^2/Pe$, the dynamics of ABPOs is faster for large $Pe$ because the MSD of their internal dynamics increases as $Pe^{4/3}$ and that of the center-of-mass motion as $Pe^2$ and, thus, exceeds that of the linear $Pe$ dependence of $D$ of APLPs as soon as $Pe \gtrsim 3(pL)^3$. In general, the MSD of active polymers with these different propulsion forces differs fundamentally, and they never exhibit the same dynamical behavior.

### D. End-to-end vector correlation function

The temporal end-to-end vector correlation functions $\langle \tilde{r}_e(t) \cdot \tilde{r}_e(0) \rangle$ and $\langle r_e(t) \cdot r_e(0) \rangle$, normalized by their equilibrium values, are
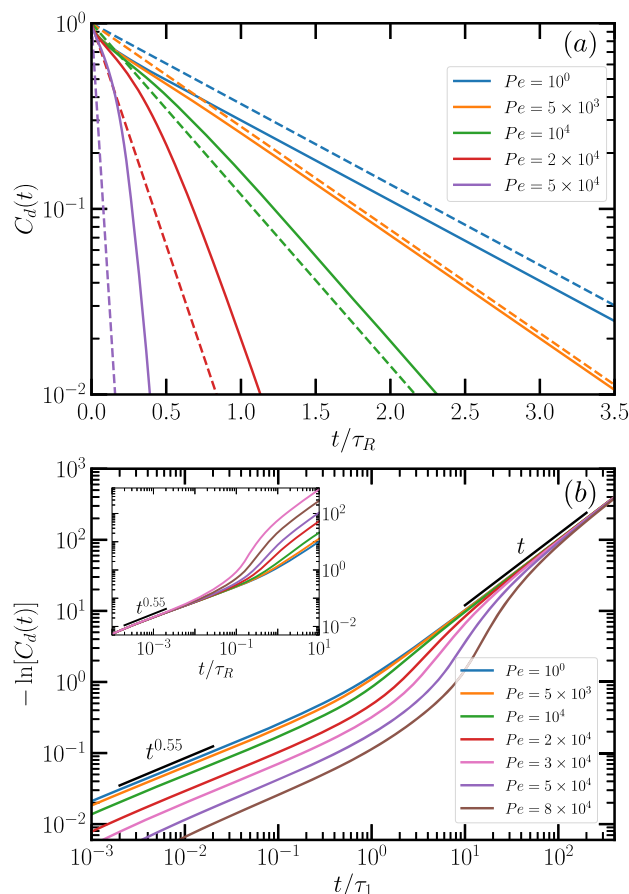
$$C_d(t) = \frac{\langle \tilde{r}_e(t) \cdot \tilde{r}_e(0) \rangle}{\langle \tilde{r}_e^2 \rangle}$$
$$= \frac{6k_BT}{Nl^2} \sum_{m,n=1}^{N} \frac{\boldsymbol{b}_m^\dagger \cdot \boldsymbol{b}_n^\dagger}{\tilde{\xi}_m + \tilde{\xi}_n} \left[ b_m^{(N)} - b_m^{(0)} \right] \left[ b_n^{(N)} - b_n^{(0)} \right] e^{-\tilde{\xi}_m t/\tilde{\gamma}}, \quad (57)$$

$$C_c(t) = \frac{\langle r_e(t) \cdot r_e(0) \rangle}{\langle r_e^2 \rangle} = \frac{16 r_c}{\pi^3} \sum_{m,n=1}^{\infty} \frac{m^2 n^2 (-1 + (-1)^m e^{-\pi r_c})(-1 + (-1)^n e^{-\pi r_c})(-1 + (-1)^{m+n} e^{2\pi r_c})}{[(m-n)^2 + 4r_c^2][(m+n)^2 + 4r_c^2](m^2 + r_c^2)(n^2 + r_c^2)} e^{-t/\tau_m}, \quad (58)$$

where $r_c = Pe/(6\pi pL)$.

Figure 10 displays end-to-end vector correlation functions for various Péclet numbers. The respective correlation functions decay approximately exponentially for $t > \tau_R$ and approach the asymptotic behavior $C_d(t) \sim e^{-t/\tau_1}$ in the limit $t \to \infty$ [Fig. 10(b)]. In the limit $t \to 0$, all $C_d(t)$ curves approach the passive asymptotic time dependence [inset of Fig. 10(b)]. The time dependence of the passive polymer crosses over from a linear regime for $t < \tau_R/N^2$ to a

compressed exponential $-\ln[C_d(t)] \sim t^{0.55}$ and finally approaches the exponential decay. The correlation functions of APLPs exhibit a $Pe$-dependent crossover from the passive polymer behavior to the asymptotic exponential decay. They decay faster with increasing $Pe$, with a significantly slower decay at short times [Fig. 10(a)]. This is clearly visible when $C_d(t)$ is presented as a function of the time $t/\tau_1$, which shows a slower decay with increasing $Pe$ before the asymptotic exponential decay is assumed. Hence, activity leads to a faster

**FIG. 10.** (a) Semi-logarithmic representation of the normalized end-to-end vector correlation function $C_d(t) = \langle \tilde{r}_e(t) \cdot \tilde{r}_e(0) \rangle / \langle \tilde{r}_e^2 \rangle$ (solid lines) as a function of the time $t/\tau_R$ for discrete APLPs of length $L/l = N = 500$ and various Péclet numbers as indicated in the legend. The dashed lines represent the correlation functions including only the longest relaxation time $\tau_1$. (b) Normalized end-to-end vector correlation function $-\ln[C_d(t)]$ as a function of the time $t/\tau_1$, where $\tau_1$ is the longest relaxation time, for various Péclet numbers. The inset shows $-\ln[C_d(t)]$ as a function of the time $t/\tau_R$. The black solid lines indicate power laws.

decorrelation of the end-to-end vector in time due to the decreasing relaxation times with increasing activity. However, larger $Pe$ lead to a slower and non-exponential decay for $t/\tau_1 \lesssim 1$.

## VI. SUMMARY AND CONCLUSIONS

We have presented analytical results for the conformational and dynamical properties of models for discrete and continuous Gaussian polymers, which are propelled by active forces along bonds for the discrete polymer and along the local tangent for the continuous polymer. The propulsion forces imply non-symmetric/non-Hermitian eigenvalue equations, which are solved by an expansion into a biorthogonal basis set. The polar nature of the polymers leads to a mode coupling in the mode amplitude correlation functions. This is in contrast to active Brownian polymers (ABPOs)[3,72] and gives rise to the emergence of distinctively different conformational and dynamical features.

Within the applied models, the polymer conformational properties are independent of the active forces and are identical to those of passive polymers. This is in contrast to ABPOs, which swell with increasing activity,[3,71,72] and some computer simulations of tangentially driven active polymers, which reveal polymer shrinkage with increasing activity.[79,81,82] However, in the latter cases, either a different propulsion force is considered and/or excluded-volume interactions are additionally taken into account. This restricts a direct comparison of the various results. Excluded-volume interactions strongly affect the conformations of active polymers. The influence is particularly strong in two dimensions as has been shown for ABPOs,[66] which shrink for small $Pe$ before they swell for large $Pe$, as well as APLPs.[79] A similar shrinkage has been observed for ABPOs in three dimensions.[67,100] Moreover, the simulation results in Ref. 82 suggest that the polymer mean-square end-to-end-distance scaling exponent $\nu$ decreases at significantly smaller $Pe$ for polymers in the presence of excluded-volume interactions than for phantom polymers. The dependence of the polymer conformations on the implementation of the applied tangential driving force is evident by comparing the simulation results of Refs. 81, 82, and 98. In Refs. 81 and 98, active driving is along bond vectors and the radius of gyration saturates at large $Pe$, whereas in Ref. 82, active driving is associated with a bead in a direction given by the unit vector connecting the positions of the leading and trailing neighbors, and the polymers continue to shrink with increasing $Pe$. Considering these aspects, further simulation studies are required to resolve the influence of the various interactions and the suitable modeling of APLPs on their conformational properties. In any case, the presented results of APLPs are consistent with simulations of active polar linear polymers in three dimensions and can qualitatively and quantitatively be compared with them for moderate active forces.

The non-symmetric matrix in the eigenvalue problem of the discrete APLPs model yields for $Pe/(6N^2) < 1$ real eigenvalues, whereas complex eigenvalues appear for $Pe/(6N^2) > 1$, with a single relaxation time and activity-dependent frequencies. These features of the active Gaussian model might appear also in simulations of slightly different models since the respective Péclet numbers are easily reached.

The coupling of modes leads to a maximum in the mode-amplitude autocorrelation function—for a continuous polymer at the mode number $m_a = \text{Integer}[Pe/(6\pi pL)]$. This requires, for the continuous polymer model, summation over an increasing number of modes with increasing $Pe$ to achieve convergence and poses a major computational difficulty for large activities.

The polymer center-of-mass mean-square displacement $\langle \Delta \tilde{r}_{cm}^2(t) \rangle$ exhibits an active ballistic time regime for $\langle \Delta \tilde{r}_{cm}^2(t) \rangle / \langle \tilde{r}_e^2 \rangle < 1$, followed by a diffusive regime with an activity-dependent diffusion coefficient, in agreement with simulations.[79,82] The effective velocity in the ballistic regime increases linearly with the Péclet number. Similarly, the effective diffusion coefficient increases linearly with $Pe$ and becomes independent of polymer length for $Pe \gg 1$, in agreement with results of computer simulations.[82] The bead mean-square displacement in the center-of-mass reference frame also shows a ballistic time regime for $t/\tilde{\tau}_R \ll 3\pi^2/Pe$ and $Pe/(6N^2) \gg 1$. The contribution of the center-of-mass motion to the total bead mean-square displacement is negligible for $\langle \Delta \tilde{r}_{tot}^2(t) \rangle / \langle \tilde{r}_e^2 \rangle < 1$, i.e., it is dominated by the active internal polymer dynamics. For $Pe \gg 1$, the diffusive dynamics is quantitatively

described by the diffusion coefficient of Eq. (50) even on length scales much smaller than $\langle \tilde{r}_e^2 \rangle$.

The dynamics of APLPs differs qualitatively from that of active Brownian polymers, where the center-of-mass motion dominates the overall polymer dynamics at large activities.[72] This reflects a complex interdependence of the dynamics of the active beads in APLPs. The active motion along the continuously changing polymer contour implies strong correlations in the bead translational motion, especially on shorter time scales.

The active dynamics of APLPs exhibits similarities to the tank-treating motion observed for active polar ring polymers (APRPs),[90] which reveal a motion along the polymer contour. This is particularly pronounced for stiff rings. Thereby, the polar nature of the linear active polymer, with a nonzero overall active force, plays an important role and leads to different time regimes compared to flexible APRPs. In particular, the long-time MSD of APRPs is independent of activity and solely determined by thermal fluctuations.

In Ref. 82, the influence of the active force on the polymer center-of-mass motion is phenomenologically described by representing it as a colored noise random process. This is similar to the active process in active Brownian polymers, whose beads or sites are indeed exposed to colored noise.[3,71] In contrast, in our approach, the dynamics of the mode-amplitudes [Eq. (14)] is governed by white noise thermal fluctuations, and the mode correlation functions decay exponentially [Eq. (34)] as for a passive polymer. The complexity of the dynamical behavior results from the tight coupling of the various modes. The difference in the noise—colored vs white —is reflected, e.g., in the dependence of the ballistic motion and active long-time diffusion on the active force, which exhibits a distinct dependence on the Péclet number, namely, linear for APLPs and quadratic for ABPOs.

Our analytical study sheds light onto the unique dynamical properties of APLPs and provides theoretical insight into yet unrevealed dependencies on activity. This will be helpful in the interpretation of experimental findings as well as the design of functional active soft matter systems.

## SUPPLEMENTARY MATERIAL

The supplementary material provides a derivation of the eigenvalues and eigenvectors of discrete APLPs, as well as the proof that the position vectors $\tilde{r}_j(t)$ are real. In addition, various definitions of conformational properties, displacements, and correlation functions are given, and derivations of approximations for the short time center-of-mass dynamics are presented. The odd–even effect in the CM-MSD of discrete APLPs at high Péclet numbers is illustrated and discussed. Movies of APLPs of length $L/l = N = 50$ and $N = 51$ exemplify the respective dynamics. Furthermore, a comparison of the total MSD of APLPs and ABPOs is performed.

## AUTHOR DECLARATIONS

### Conflict of Interest

The authors have no conflicts to disclose.

### Author Contributions

**Christian A. Philipps**: Formal analysis (equal); Investigation (equal); Writing – original draft (equal); Writing – review & editing (equal). **Gerhard Gompper**: Conceptualization (supporting); Project administration (equal); Supervision (equal); Writing – review & editing (equal). **Roland G. Winkler**: Conceptualization (lead); Project administration (equal); Supervision (equal); Writing – original draft (equal); Writing – review & editing (equal).

## DATA AVAILABILITY

The data that support the findings of this study are available from the corresponding author upon reasonable request.

## REFERENCES

[1] Y. Demirel, "Nonequilibrium thermodynamics modeling of coupled biochemical cycles in living cells," J. Non-Newtonian Fluid Mech. **165**, 953 (2010).

[2] X. Fang, K. Kruse, T. Lu, and J. Wang, "Nonequilibrium physics in biology," Rev. Mod. Phys. **91**, 045004 (2019).

[3] R. G. Winkler and G. Gompper, "The physics of active polymers and filaments," J. Chem. Phys. **153**, 040901 (2020).

[4] R. Kapral, "Perspective: Nanomotors without moving parts that propel themselves in solution," J. Chem. Phys. **138**, 020901 (2013).

[5] A. W. C. Lau, B. D. Hoffman, A. Davies, J. C. Crocker, and T. C. Lubensky, "Microrheology, stress fluctuations, and active behavior of living cells," Phys. Rev. Lett. **91**, 198101 (2003).

[6] C. P. Brangwynne, G. H. Koenderink, F. C. MacKintosh, and D. A. Weitz, "Cytoplasmic diffusion: Molecular motors mix it up," J. Cell Biol. **183**, 583 (2008).

[7] D. Robert, T.-H. Nguyen, F. Gallet, and C. Wilhelm, "In vivo determination of fluctuating forces during endosome trafficking using a combination of active and passive microrheology," PLoS One **5**, e10046 (2010).

[8] N. Fakhri, A. D. Wessel, C. Willms, M. Pasquali, D. R. Klopfenstein, F. C. MacKintosh, and C. F. Schmidt, "High-resolution mapping of intracellular fluctuations using carbon nanotubes," Science **344**, 1031 (2014).

[9] M. Guo, A. J. Ehrlicher, M. H. Jensen, M. Renz, J. R. Moore, R. D. Goldman, J. Lippincott-Schwartz, F. C. Mackintosh, and D. A. Weitz, "Probing the stochastic, motor-driven properties of the cytoplasm using force spectrum microscopy," Cell **158**, 822 (2014).

[10] B. R. Parry, I. V. Surovtsev, M. T. Cabeen, C. S. O'Hern, E. R. Dufresne, and C. Jacobs-Wagner, "The bacterial cytoplasm has glass-like properties and is fluidized by metabolic activity," Cell **156**, 183 (2014).

[11] R. Golestanian, "Enhanced diffusion of enzymes that catalyze exothermic reactions," Phys. Rev. Lett. **115**, 108102 (2015).

[12] A. S. Mikhailov and R. Kapral, "Hydrodynamic collective effects of active protein machines in solution and lipid bilayers," Proc. Natl. Acad. Sci. U. S. A. **112**, E3639 (2015).

[13] S. C. Weber, A. J. Spakowitz, and J. A. Theriot, "Nonthermal ATP-dependent fluctuations contribute to the in vivo motion of chromosomal loci," Proc. Natl. Acad. Sci. U. S. A. **109**, 7338 (2012).

[14] R. Kapral and A. S. Mikhailov, "Stirring a fluid at low Reynolds numbers: Hydrodynamic collective effects of active proteins in biological cells," Physica D **318-319**, 100 (2016).

[15] F. S. Gnesotto, F. Mura, J. Gladrow, and C. P. Broedersz, "Broken detailed balance and non-equilibrium dynamics in living systems: A review," Rep. Prog. Phys. **81**, 066601 (2018).

[16] F. Wu, A. Japaridze, X. Zheng, J. Wiktor, J. W. J. Kerssemakers, and C. Dekker, "Direct imaging of the circular chromosome in a live bacterium," Nat. Commun. **10**, 2194 (2019).

[17] F. C. MacKintosh and A. J. Levine, "Nonequilibrium mechanics and dynamics of motor-activated gels," Phys. Rev. Lett. **100**, 018104 (2008).

[18] W. Lu, M. Winding, M. Lakonishok, J. Wildonger, and V. I. Gelfand, "Microtubule–microtubule sliding by kinesin-1 is essential for normal cytoplasmic streaming in *Drosophila* oocytes," Proc. Natl. Acad. Sci. U. S. A. **113**, E4995 (2016).

[19]A. Ravichandran, G. A. Vliegenthart, G. Saggiorato, T. Auth, and G. Gompper, "Enhanced dynamics of confined cytoskeletal filaments driven by asymmetric motors," Biophys. J. **113**, 1121 (2017).

[20]M. Guthold, X. Zhu, C. Rivetti, G. Yang, N. H. Thomson, S. Kasas, H. G. Hansma, B. Smith, P. K. Hansma, and C. Bustamante, "Direct observation of one-dimensional diffusion and transcription by *Escherichia coli* RNA polymerase," Biophys. J. **77**, 2284 (1999).

[21]Y. X. Mejia, E. Nudler, and C. Bustamante, "Trigger loop folding determines transcription rate of *Escherichia coli's* RNA polymerase," Proc. Natl. Acad. Sci. U. S. A. **112**, 743 (2015).

[22]V. Belitsky and G. M. Schütz, "Stationary RNA polymerase fluctuations during transcription elongation," Phys. Rev. E **99**, 012405 (2019).

[23]A. Javer, Z. Long, E. Nugent, M. Grisi, K. Siriwatwetchakul, K. D. Dorfman, P. Cicuta, and M. Cosentino Lagomarsino, "Short-time movement of *E. coli* chromosomal loci depends on coordinate and subcellular localization," Nat. Commun. **4**, 3003 (2013).

[24]A. Zidovska, D. A. Weitz, and T. J. Mitchison, "Micron-scale coherence in interphase chromatin dynamics," Proc. Natl. Acad. Sci. U. S. A. **110**, 15555 (2013).

[25]E. Lieberman-Aiden, N. L. van Berkum, L. Williams, M. Imakaev, T. Ragoczy, A. Telling, I. Amit, B. R. Lajoie, P. J. Sabo, M. O. Dorschner, R. Sandstrom, B. Bernstein, M. A. Bender, M. Groudine, A. Gnirke, J. Stamatoyannopoulos, L. A. Mirny, E. S. Lander, and J. Dekker, "Comprehensive mapping of long-range interactions reveals folding principles of the human genome," Science **326**, 289 (2009).

[26]T. Cremer, M. Cremer, B. Hübner, H. Strickfaden, D. Smeets, J. Popken, M. Sterr, Y. Markaki, K. Rippe, and C. Cremer, "The 4D nucleome: Evidence for a dynamic nuclear landscape based on co-aligned active and inactive nuclear compartments," FEBS Lett. **589**, 2931 (2015).

[27]I. Solovei, K. Thanisch, and Y. Feodorova, "How to rule the nucleus: Divide et impera," Curr. Opin. Cell Biol. **40**, 47 (2016).

[28]D. Saintillan, M. J. Shelley, and A. Zidovska, "Extensile motor activity drives coherent motions in a model of interphase chromatin," Proc. Natl. Acad. Sci. U. S. A. **115**, 11442 (2018).

[29]N. Ganai, S. Sengupta, and G. I. Menon, "Chromosome positioning from activity-based segregation," Nucleic Acids Res. **42**, 4145 (2014).

[30]J. Smrek and K. Kremer, "Small activity differences drive phase separation in active-passive polymer mixtures," Phys. Rev. Lett. **118**, 098002 (2017).

[31]R. Kawamura, A. Kakugo, K. Shikinaka, Y. Osada, and J. P. Gong, "Ring-shaped assembly of microtubules shows preferential counterclockwise motion," Biomacromolecules **9**, 2277 (2008).

[32]B. Liu, T. R. Powers, and K. S. Breuer, "Force-free swimming of a model helical flagellum in viscoelastic fluids," Proc. Natl. Acad. Sci. U. S. A. **108**, 19516 (2011).

[33]J. J. Keya, A. M. R. Kabir, and A. Kakugo, "Synchronous operation of biomolecular engines," Biophys. Rev. **12**, 401 (2020).

[34]T. Butt, T. Mufti, A. Humayun, P. B. Rosenthal, S. Khan, S. Khan, and J. E. Molloy, "Myosin motors drive long range alignment of actin filaments," J. Biol. Chem. **285**, 4964 (2010).

[35]V. Schaller, C. Weber, C. Semmrich, E. Frey, and A. R. Bausch, "Polar patterns of driven filaments," Nature **467**, 73 (2010).

[36]V. Schaller, C. Weber, E. Frey, and A. R. Bausch, "Polar pattern formation: Hydrodynamic coupling of driven filaments," Soft Matter **7**, 3213 (2011).

[37]A. Doostmohammadi, J. Ignés-Mullol, J. M. Yeomans, and F. Sagués, "Active nematics," Nat. Commun. **9**, 3246 (2018).

[38]T. Sanchez, D. T. N. Chen, S. J. DeCamp, M. Heymann, and Z. Dogic, "Spontaneous motion in hierarchically assembled active matter," Nature **491**, 431 (2012).

[39]D. Needleman and Z. Dogic, "Active matter at the interface between materials science and cell biology," Nat. Rev. Mater. **2**, 17048 (2017).

[40]G. A. Vliegenthart, A. Ravichandran, M. Ripoll, T. Auth, and G. Gompper, "Filamentous active matter: Band formation, bending, buckling, and defects," Sci. Adv. **6**, eaaw9975 (2020).

[41]R. Alert, J.-F. Joanny, and J. Casademunt, "Universal scaling of active nematic turbulence," Nat. Phys. **16**, 682 (2020).

[42]B. Martínez-Prat, R. Alert, F. Meng, J. Ignés-Mullol, J.-F. Joanny, J. Casademunt, R. Golestanian, and F. Sagués, "Scaling regimes of active turbulence with external dissipation," Phys. Rev. X **11**, 031065 (2021).

[43]Y. Sasaki, Y. Takikawa, V. S. R. Jampani, H. Hoshikawa, T. Seto, C. Bahr, S. Herminghaus, Y. Hidaka, and H. Orihara, "Colloidal caterpillars for cargo transportation," Soft Matter **10**, 8813 (2014).

[44]F. Martinez-Pedrero, A. Ortiz-Ambriz, I. Pagonabarraga, and P. Tierno, "Colloidal microworms propelling via a cooperative hydrodynamic conveyor belt," Phys. Rev. Lett. **115**, 138301 (2015).

[45]J. Yan, M. Han, J. Zhang, C. Xu, E. Luijten, and S. Granick, "Reconfiguring active particles by electrostatic imbalance," Nat. Mater. **15**, 1095 (2016).

[46]R. Di Leonardo, "Active colloids: Controlled collective motions," Nat. Mater. **15**, 1057 (2016).

[47]J. Zhang, J. Yan, and S. Granick, "Directed self-assembly pathways of active colloidal clusters," Angew. Chem., Int. Ed. **55**, 5166 (2016).

[48]J. Zhang and S. Granick, "Natural selection in the colloid world: Active chiral spirals," Faraday Discuss. **191**, 35 (2016).

[49]H. R. Vutukuri, B. Bet, R. van Roij, M. Dijkstra, and W. T. S. Huck, "Rational design and dynamics of self-propelled colloidal bead chains: From rotators to flagella," Sci. Rep. **7**, 16758 (2017).

[50]G. Kokot, S. Das, R. G. Winkler, G. Gompper, I. S. Aranson, and A. Snezhko, "Active turbulence in a gas of self-assembled spinners," Proc. Natl. Acad. Sci. U. S. A. **114**, 12870 (2017).

[51]B. Biswas, R. K. Manna, A. Laskar, P. B. S. Kumar, R. Adhikari, and G. Kumaraswamy, "Linking catalyst-coated isotropic colloids into 'active' flexible chains enhances their diffusivity," ACS Nano **11**, 10025 (2017).

[52]D. Nishiguchi, J. Iwasawa, H.-R. Jiang, and M. Sano, "Flagellar dynamics of chains of active Janus particles fueled by an AC electric field," New J. Phys. **20**, 015002 (2018).

[53]H. Löwen, "Active colloidal molecules," Europhys. Lett. **121**, 58001 (2018).

[54]M. Shafiei Aporvari, M. Utkur, E. U. Saritas, G. Volpe, and J. Stenhammar, "Anisotropic dynamics of a self-assembled colloidal chain in an active bath," Soft Matter **16**, 5609 (2020).

[55]J. R. Howse, R. A. L. Jones, A. J. Ryan, T. Gough, R. Vafabakhsh, and R. Golestanian, "Self-motile colloidal particles: From directed propulsion to random walk," Phys. Rev. Lett. **99**, 048102 (2007).

[56]H.-R. Jiang, N. Yoshinaga, and M. Sano, "Active motion of a Janus particle by self-thermophoresis in a defocused laser beam," Phys. Rev. Lett. **105**, 268302 (2010).

[57]L. F. Valadares, Y.-G. Tao, N. S. Zacharia, V. Kitaev, F. Galembeck, R. Kapral, and G. A. Ozin, "Catalytic nanomotors: Self-propelled sphere dimers," Small **6**, 565–572 (2010).

[58]A. Würger, "Thermal non-equilibrium transport in colloids," Rep. Prog. Phys. **73**, 126601 (2010).

[59]G. Volpe, I. Buttinoni, D. Vogt, H.-J. Kümmerer, and C. Bechinger, "Microswimmers in patterned environments," Soft Matter **7**, 8810 (2011).

[60]S. Thutupalli, R. Seemann, and S. Herminghaus, "Swarming behavior of simple model squirmers," New J. Phys. **13**, 073021 (2011).

[61]I. Buttinoni, J. Bialké, F. Kümmel, H. Löwen, C. Bechinger, and T. Speck, "Dynamical clustering and phase separation in suspensions of self-propelled colloidal particles," Phys. Rev. Lett. **110**, 238301 (2013).

[62]B. ten Hagen, F. Kümmel, R. Wittkowski, D. Takagi, H. Löwen, and C. Bechinger, "Gravitaxis of asymmetric self-propelled colloidal particles," Nat. Commun. **5**, 4829 (2014).

[63]C. Bechinger, R. Di Leonardo, H. Löwen, C. Reichhardt, G. Volpe, and G. Volpe, "Active particles in complex and crowded environments," Rev. Mod. Phys. **88**, 045006 (2016).

[64]C. C. Maass, C. Krüger, S. Herminghaus, and C. Bahr, "Swimming droplets," Annu. Rev. Condens. Matter Phys. **7**, 171 (2016).

[65]J. Harder, C. Valeriani, and A. Cacciuto, "Activity-induced collapse and reexpansion of rigid polymers," Phys. Rev. E **90**, 062312 (2014).

[66]A. Kaiser and H. Löwen, "Unusual swelling of a polymer in a bacterial bath," J. Chem. Phys. **141**, 044903 (2014).

[67]S. K. Anand and S. P. Singh, "Conformation and dynamics of a self-avoiding active flexible polymer," Phys. Rev. E **101**, 030501 (2020).

[68]S. Das, N. Kennedy, and A. Cacciuto, "The coil–globule transition in self-avoiding active polymers," Soft Matter **17**, 160 (2021).

[69]A. Ghosh and N. S. Gov, "Dynamics of active semiflexible polymers," Biophys. J. **107**, 1065 (2014).

[70]J. Shin, A. G. Cherstvy, W. K. Kim, and R. Metzler, "Facilitation of polymer looping and giant polymer diffusivity in crowded solutions of active particles," New J. Phys. **17**, 113008 (2015).

[71]T. Eisenstecken, G. Gompper, and R. G. Winkler, "Conformational properties of active semiflexible polymers," Polymers **8**, 304 (2016).

[72]T. Eisenstecken, G. Gompper, and R. G. Winkler, "Internal dynamics of semiflexible polymers with active noise," J. Chem. Phys. **146**, 154903 (2017).

[73]A. Martín-Gómez, G. Gompper, and R. G. Winkler, "Active Brownian filamentous polymers under shear flow," Polymers **10**, 837 (2018).

[74]S. M. Mousavi, G. Gompper, and R. G. Winkler, "Active Brownian ring polymers," J. Chem. Phys. **150**, 064913 (2019).

[75]A. Suma, G. Gonnella, D. Marenduzzo, and E. Orlandini, "Motility-induced phase separation in an active dumbbell fluid," Europhys. Lett. **108**, 56004 (2014).

[76]J. T. Siebert, J. Letz, T. Speck, and P. Virnau, "Phase behavior of active Brownian disks, spheres, and dimers," Soft Matter **13**, 1020 (2017).

[77]A. Martin-Gomez, T. Eisenstecken, G. Gompper, and R. G. Winkler, "Hydrodynamics of polymers in an active bath," Phys. Rev. E **101**, 052612 (2020).

[78]A. Martín-Gómez, T. Eisenstecken, G. Gompper, and R. G. Winkler, "Active Brownian filaments with hydrodynamic interactions: Conformations and dynamics," Soft Matter **15**, 3957 (2019).

[79]R. E. Isele-Holder, J. Elgeti, and G. Gompper, "Self-propelled worm-like filaments: Spontaneous spiral formation, structure, and dynamics," Soft Matter **11**, 7181 (2015).

[80]Ö. Duman, R. E. Isele-Holder, J. Elgeti, and G. Gompper, "Collective dynamics of self-propelled semiflexible filaments," Soft Matter **14**, 4483 (2018).

[81]S. K. Anand and S. P. Singh, "Structure and dynamics of a self-propelled semiflexible filament," Phys. Rev. E **98**, 042501 (2018).

[82]V. Bianco, E. Locatelli, and P. Malgaretti, "Globulelike conformation and enhanced diffusion of active polymers," Phys. Rev. Lett. **121**, 217802 (2018).

[83]K. R. Prathyusha, S. Henkes, and R. Sknepnek, "Dynamically generated patterns in dense suspensions of active filaments," Phys. Rev. E **97**, 022606 (2018).

[84]M. Foglino, E. Locatelli, C. A. Brackley, D. Michieletto, C. N. Likos, and D. Marenduzzo, "Non-equilibrium effects of molecular motors on polymers," Soft Matter **15**, 5995 (2019).

[85]J. M. Moore, T. N. Thompson, M. A. Glaser, and M. D. Betterton, "Collective motion of driven semiflexible filaments tuned by soft repulsion and stiffness," Soft Matter **16**, 9436 (2020).

[86]M. S. E. Peterson, M. F. Hagan, and A. Baskaran, "Statistical properties of a tangentially driven active filament," J. Stat. Mech.: Theory Exp. **2020**, 013216.

[87]C. Nguyen, Y. Ozkan-Aydin, H. Tuazon, D. I. Goldman, M. S. Bhamla, and O. Peleg, "Emergent collective locomotion in an active polymer model of entangled worm blobs," Front. Phys. **9**, 734499 (2021).

[88]E. Locatelli, V. Bianco, and P. Malgaretti, "Activity-induced collapse and arrest of active polymer rings," Phys. Rev. Lett. **126**, 097801 (2021).

[89]L. Qiao and R. Kapral, "Control of active polymeric filaments by chemically powered nanomotors," Phys. Rev. Applied **18**, 024051 (2022).

[90]C. A. Philipps, G. Gompper, and R. G. Winkler, "Dynamics of active polar ring polymers," Phys. Rev. E **105**, L062501 (2022).

[91]L. Harnau, R. G. Winkler, and P. Reineker, "Dynamic properties of molecular chains with variable stiffness," J. Chem. Phys. **102**, 7750 (1995).

[92]M. Doi and S. F. Edwards, *The Theory of Polymer Dynamics* (Clarendon Press, Oxford, 1986).

[93]R. G. Winkler, P. Reineker, and L. Harnau, "Models and equilibrium properties of stiff molecular chains," J. Chem. Phys. **101**, 8119–8129 (1994).

[94]R. G. Winkler, "Deformation of semiflexible chains," J. Chem. Phys. **118**, 2919 (2003).

[95]H. Risken, *Fokker-Planck Equation: Methods of Solution and Applications* (Springer-Verlag, 1984).

[96]B. Y. Ha and D. Thirumalai, "A mean-field model for semiflexible chains," J. Chem. Phys. **103**, 9408 (1995).

[97]C. Battle, C. P. Broedersz, N. Fakhri, V. F. Geyer, J. Howard, C. F. Schmidt, and F. C. MacKintosh, "Broken detailed balance at mesoscopic scales in active biological systems," Science **352**, 604 (2016).

[98]M. Fazelzadeh, E. Irani, Z. Mokhtari, and S. Jabbari-Farouji, "Effects of inertia on conformation and dynamics of active filaments," arXiv:2209.07880 (2022).

[99]J. Elgeti, R. G. Winkler, and G. Gompper, "Physics of microswimmers—Single particle motion and collective behavior: A review," Rep. Prog. Phys. **78**, 056601 (2015).

[100]T. Eisenstecken, A. Ghavami, A. Mair, G. Gompper, and R. G. Winkler, "Conformational and dynamical properties of semiflexible polymers in the presence of active noise," AIP Conf. Proc. **1871**, 050001 (2017).